Rapid and simultaneous estimation of fault slip and heterogeneous lithospheric viscosity from postseismic deformation

Trever T. Hines and Eric A. Hetland

March 24, 2015

1 Abstract

2 Introduction

Geodetic observations of surface deformation in the months to years following an earthquake are often attributed to afterslip (e.g. *Marone et al.*, 1991), viscoelastic relaxation in the lithosphere (e.g. *Nur & Mavko*, 1974), and/or poroelastic-relaxation (e.g. *Peltzer et al.*, 1998; *Jónsson et al.*, 2003). If postseismic deformation can be entirely described by afterslip, then one could easily constrain the spatial distribution of fault slip with a linear least squares inversion (e.g. *Freed*, 2007; *Bürgmann et al.*, 2002; *Harris & Segall*, 1987), which could then provide insight into the frictional properties of faults (e.g. *Hsu et al.*, 2006; *Barbot et al.*, 2009). However, postseismic deformation following large (Mw$\geq$7) earthquakes is often attributed to viscoelastic relaxation in the lithosphere (e.g. *Pollitz*, 2003, 2005; *Hetland & Hager*, 2003) or a combination of both afterslip and viscoelastic relaxation (e.g. *Johnson et al.*, 2009; *Freed et al.*, 2006; *Hearn et al.*, 2008; *Rollins et al.*, 2015). In such cases, postseismic

deformation can be used to constrain the viscous properties of the lithosphere, although this is a more difficult task than constraining a slip distribution. Not only are there potentially competing deformation mechanism which must be discerned, finding the viscosity of the lithopshere from postseimsic deformation is a computationally expensive nonlinear inverse problem. Typically, this is approached with a forward modeling, grid search method. These forward modeling techniques require the number of unknown parameters being estimated to be small, meaning that significant and potentially inappropriate modeling assumptions must be made (*Hines & Hetland*, 2013; *Riva & Govers*, 2008).

In this paper we propose a relatively fast method to kinematically invert coseismic and postseismic deformation to simultaneously estimate a time-dependent distribution of fault slip and an arbitrarily discretized viscosity structure of the lithosphere. Our method is based on an approximation which linearizes the rate of early postseismic deformation with respect to the viscosity of the lithosphere. We demonstrate the efficacy and limitations of our method through a synthetic test.

3 Linearizing early postseismic deformation

We assume that the lithosphere can be approximated as a Maxwell viscoelastic material on the timescales of postseismic deformation, where shear stress and strain are related by

$$\frac{\partial \varepsilon}{\partial t} = \frac{\sigma}{2\eta} + \frac{1}{2\mu}\frac{\partial \sigma}{\partial t}. \tag{1}$$

η and μ are viscosity and shear modulus, respectively. This constitutive relationship implies that a sudden strain in the lithosphere from an earthquake will instantaneously propagate stresses through the lithosphere elastically (assuming the lithosphere is undergoing quasi-static deformation). Creep will also initiate immediately after the earthquake, where the initial viscous strain rate in each parcel of the lithosphere will be proportional to the fluidity ($\varphi = 1/\eta$) in that parcel, and independent of the fluidity elsewhere. Each parcel will

continue to creep at approximately that rate for as long as the initial elastic stresses from the earthquake are large compared to the stresses transferred throughout the lithosphere by viscoelastic relaxation. In this early postseismic period, creep in each parcel will express itself as surface deformation with an amplitude that is also proportional to the fluidity in that parcel and independent of the fluidity elsewhere. The early surface expression of creep in the entire lithosphere is therefore a sum of the surface expression of each parcel and is linear with respect to lithospheric fluidity. This property of early postseismic surface deformation is demonstrated below using simple infinite length, strike-slip earthquake models, where the lithosphere is approximated as a layered halfspace. We use the linearity of postseismic deformation with respect to fluidity to greatly facilitates the inverse problem of estimating lithospheric viscosity.

3.1 Two-dimensional earthquake models

The easiest way to demonstrate how postseismic deformation can be linearized with respect to lithospheric viscosity is with a simple two-dimensional earthquake model consisting of a long, vertical, surface rupturing, strike-slip fault oriented in the anti-plane direction and embedded in a viscoelastic horizontal layer overlying a viscoelastic halfspace. We make use of the correspondence principle of viscoelasticity (e.g. *Flügge*, 1975), which states that the Laplace transform of deformation in a viscoelastic body has the same form as the Laplace transform of deformation in a elastic body with the same geometry and subjected to the same boundary conditions. The solution for displacements following an earthquake in a viscoelastic lithosphere can then be easily found provided that the solution for displacements in an elastic lithosphere with the same geometry is known (e.g. *Hetland & Hager*, 2005; *Nur & Mavko*, 1974; *Savage & Prescott*, 1978). One only needs to replace the shear modulus in the Laplace transform of the elastic solution with the effective viscoelastic shear modulus and then compute the inverse Laplace transform.

3.1.1 Two layered model

From the solution of *Rybicki* (1971), surface displacements, $u_e(x,t)$, resulting from slip on a fault in an elastic surface layer overlying a semi-infinite elastic substrate are

$$u_e(x,t) = b(t)\left(\frac{1}{2}W(0) + \sum_{n=1}^{\infty}\Gamma^n W(n)\right), \tag{2}$$

where

$$W(n) = \frac{1}{\pi}\left(\tan^{-1}\left(\frac{2nH+D}{x}\right) - \tan^{-1}\left(\frac{2nH-D}{x}\right)\right), \tag{3}$$

and

$$\Gamma = \frac{\mu_1 - \mu_2}{\mu_1 + \mu_2}. \tag{4}$$

In the above equation, $b(t)$ describes cummulative slip on the fault over time and can describe coseismic slip and/or afterslip. D is the locking depth of the fault, H is the thickness of the upper layer, while μ_1 and μ_2 are the shear modulii in the upper layer and lower substrate, respectively.

We take the Laplace transform of eq (2),

$$\hat{u}_e(x,s) = \hat{b}(s)\left(\frac{1}{2}W(0) + \sum_{n=1}^{\infty}\Gamma^n W(n)\right), \tag{5}$$

then find the Laplace transform of surface displacements in the two-layered, viscoelastic half-space by replacing μ_1 and μ_2 with the equivalent shear modulii for Maxwell materials in the Laplace domain, $\hat{\mu}_1$ and $\hat{\mu}_2$, which is

$$\hat{u}_v(x,s) = \hat{b}(s)\left(\frac{1}{2}W(0) + \sum_{n=1}^{\infty}\hat{\Gamma}^n W(n)\right), \tag{6}$$

where

$$\hat{\Gamma} = \frac{\hat{\mu_1} - \hat{\mu_2}}{\hat{\mu_1} + \hat{\mu_2}}, \tag{7}$$

$$\hat{\mu_1} = \frac{s}{\frac{s}{\mu_1} + \frac{1}{\eta_1}}, \tag{8}$$

and

$$\hat{\mu_2} = \frac{s}{\frac{s}{\mu_2} + \frac{1}{\eta_2}}. \tag{9}$$

To find the surface displacements in the time domain one must find the inverse Lapace transform of eq (6), which is typically done using the method of residues (e.g. *Nur & Mavko*, 1974). However, we are interested in characterizing the behavior of early postseismic deformation and it better serves us to instead perform the inverse Laplace transform with an extension of the initial value theorem (Appendix A).

For simplicity, we assume below that the shear modulus for the viscoelastic lithosphere is homogenous throughout the lithosphere (i.e. $\mu_1 = \mu_2$), although we demonstrate in a supplementary ipython notebook that our conclusions still hold when $\mu_1 \neq \mu_2$. The surface displacements in the time domain are

$$u_v(x,t) = b(t)\frac{1}{2}W(0) + b(t) * \mathcal{L}^{-1}\left[\sum_{n=1}^{\infty} \hat{\Gamma}^n W(n)\right]. \tag{10}$$

Evaluating the above inverse Laplace transform using the method described in Appendix A:

$$\begin{aligned} u_v(x,t) =& b(t)\frac{1}{2}W(0) + \\ & b(t) * \left(\frac{\mu}{2\eta_2}W(1) - \frac{\mu}{2\eta_1}W(1)\right) + \\ & b(t) * \left(\left(\frac{\mu^2 t}{4\eta_2^2} - \frac{\mu^2 t}{4\eta_1\eta_2}\right)(W(1) - W(2)) + \left(\frac{\mu^2 t}{4\eta_1\eta_2} - \frac{\mu^2 t}{4\eta_1^2}\right)(W(1) + W(2))\right) + \\ & \ldots . \end{aligned} \tag{11}$$

The first term in eq (11) is the surface displacement resulting from the elastic transfer of stresses created by slip on the fault. The remaining terms are a Taylor series expansion of surface deformation resulting from viscoelastic relaxation. The first of these remaining term, describing the initial viscoelastic response, is a linear expression with respect to the fluidity in each of the two layers.

If the time since the rupture is sufficiently small compared to the relaxation times of each layer, $\tau_i = \eta_i/\mu$, (i.e. the third and following terms in eq. (11) are small), then we can truncate the series and approximate early surface deformation using only the elastic response and the initial viscoelastic response

$$u_v(x,t) \approx b(t)\frac{1}{2}W(0) + \int_0^t b(\theta)\left(\frac{\mu}{2\eta_2}W(1) - \frac{\mu}{2\eta_1}W(1)\right)d\theta. \tag{12}$$

In Section 3.1 we express eq. (12) in a more general form which allows for an arbitrarily discretized lithosphere. It is therefore valuable to explore the quality of the above approximation for this simple two layered case. Figure 1 shows the series solution from eq. (11) truncated at a sufficiently large N as well as the approximation given by eq. (12). In this comparison, we use a shear modulus of 32.0 GPa throughout the lithosphere, viscosities 10^{20} and 10^{19} Pa s for the top layer and lower half-space, respectively, and we let b(t) describe 5.0 m of instantaneous slip at $t = 0.0$. It should be noted that a similar approximation was demonstrated by *Segall* (2010) for an elastic layer over a Maxwell viscoelastic half-space. The approximate solution coincides with the series expansion up until about 6 years after the earthquake. At that point, the approximation begins to appreciably overestimate the series solution. In our experience the approximate given by (12) is accurate for about as long as the relaxation time of the weakest layer, which is 10 years in this case.

It is worth noting that the initial viscoelastic response for the uppermost layer and lower half-space differ only in sign and in amplitude. In the context of an inverse problem, this means that it is impossible to use (12) to estimate the absolute viscosity of the two

layers, rather it is only possible to estimate their relative viscosities. This is not a difficult obstacle to overcome because in application we can typically assume that the upper layer has a sufficiently long Maxwell relaxation time such that it is effectively elastic over the postseismic period.

3.1.2 Three layered model

We follow the same procedure from above to find the surface deformation resulting from slip on a strike-slip fault in a three layered viscoelastic half-space. Starting from the layered elastic solution from *Chinnery & Jovanovich* (1972), we evalutate the solution for the viscoelastic problem in our supplementary ipython notebook. Once again, we find that the initial viscoelastic response is linear with respect to the fluidity in each of the three layers and we approximate early postseismic deformation resulting from slip described by $b(t)$ as

$$u_v(x,t) \approx b(t)\frac{1}{2}W(0,0) + \int_0^t b(\theta)\left(\frac{\mu}{2\eta_3}W(1,1) + \frac{\mu}{2\eta_2}(W(0,1) - W(1,1)) - \frac{\mu}{2\eta_1}W(0,1)\right)d\theta, \tag{13}$$

where

$$W(n,m) = \frac{1}{\pi}\left(\tan^{-1}\left(\frac{2nH_2 + 2mH_1 + D}{x}\right) - \tan^{-1}\left(\frac{2nH_2 + 2mH_1 - D}{x}\right)\right), \tag{14}$$

η_1, η_2, and η_3 are the viscosities of the top, middle, and bottom layers, respectively, and H_1 and H_2 are the thicknesses of the top and middle layer, respectively. We can see that eq. (13) recovers eq. (12) when $\eta_3 = \eta_2$.

3.1.3 Continuous depth dependent model

At this point we posit that a similar approximation can be made for an arbitrarily layered lithosphere, at least for the two-dimensional case. With this assumption, we can then use eq. (13) to find an initial viscoelastic response kernel and then integrate that kernel over

the depth of the lithosphere to find the initial viscoelastic response for an arbitrary depth dependent viscosity structure. If the lithsophere is elastic above the fault depth, D, and described by $\eta(z)$ below D then early postseismic deformation can be approximated as

$$u(x,t) \approx \frac{b(t)}{\pi}\tan^{-1}(\frac{D}{x}) + \int_o^t \int_D^\infty \frac{\mu b(\theta)}{2\pi\eta(\zeta)} \left(\frac{2x}{x^2 + (D+2\zeta)^2} - \frac{2x}{x^2 + (2\zeta - D)^2} \right) d\zeta d\theta. \quad (15)$$

Although the above equation is capable of describing an arbitrary depth dependent viscosity structure, it falls short of being useful as the forward solution in an inverse problem aimed at estimating lithospheric viscosity. This is because the above equation makes the unphysical assumption that the fault is infinitely long. This would introduce first order errors, which would likely wash out the second order effect of viscosity. We use eq. (15) for making estimates of the depth sensitivity of postseismic deformation.

3.2 arbitrarily discretized earthquake models

Motivated by our above results, we make the assertion that the initial rate of surface deformation resulting from an instantaneous dislocation in a three-dimensional Maxwell viscoelastic medium, which has been arbitrarily discretized into N regions, will have the form

$$\frac{\partial}{\partial t} u(x,t)\big|_{t=0} = \sum_j^N \frac{1}{\eta_j} G_j(x). \quad (16)$$

$G_j(x)$ is the initial rate of surface deformation resulting from viscous creep when there is unit fluidity in region j and fluidity is zero (i.e. elastic) in all other regions. In this sense, $G_j(x)$ can be thought of as a Green's function for the initial rate of surface deformation resulting for viscoelastic deformation and thus we refer to $G_j(x)$ as the initial viscoelastic Green's function. We verify eq. (16) numerically in section 5.5 and save a theoretical justification for a later paper.

We can then approximate surface deformation as

$$u(x,t) \approx b(t)F(x) + \sum_{j}^{N} \int_{0}^{t} \frac{b(\theta)}{\eta_j} G_j(x) d\theta, \tag{17}$$

where $F(x)$ is the elastic Green's function, which describes the elastic deformation resulting from a dislocation with a unit of slip.

We further generalize this approximation of surface deformation to allow for an arbitrary spatial distribution of slip by using linear superposition. If the elastic defomation in a viscoelastic lithosphere can be described in terms of M elastic dislocation sources, then early surface deformation resulting from both elastic dislocations and viscous creep can be approximated as

$$u(x,t) \approx \sum_{i}^{M} b_i(t)F_i(x) + \sum_{i}^{M}\sum_{j}^{N} \int_{0}^{t} \frac{b_i(\theta)}{\eta_j} G_{ij}(x) d\theta. \tag{18}$$

The initial viscoelastic Green's function is dependent upon both the region it represents as well as the dislocation source which induces the viscous creep in that region, hence the two indices.

It is worth noting that the approximation given above does not account for the viscoelastic coupling between the regions since each region's contribution to surface deformation is independent of the viscosity elsewhere. This approximation is therfore appropriate for as long as the regions do not significantly transfer stresses between eachother through viscoelastic deformation.

4 Inversion method

The approximation of postseismic deformation given by eq. (18) can be cast as an inverse problem aimed at finding the distribution of slip on a fault and an arbitrarily complicated lithosphere viscosity structure from postseismic deformation. We assume that the slip history

in any one direction on each fault patch, $b_i(t)$, can be expressed as P linear terms such that

$$b_i(t) = \sum_{k}^{P} \alpha_{ik} A_k(t). \tag{19}$$

In this paper, $A_k(t)$ consists of either step functions, which describe coseismic slip on a fault patch, or ramp functions, which describe afterslip on a fault patch over a time interval. The approximation given by eq. (18) now becomes

$$u(x,t) \approx \sum_{i}^{M} \sum_{k}^{P} \alpha_{ik} F_i(x) A_k(t) + \sum_{i}^{M} \sum_{j}^{N} \sum_{k}^{P} \int_0^t \frac{\alpha_{ik}}{\eta_j} G_{ij}(x) A_k(\theta) d\theta. \tag{20}$$

If we assume a fault geometry and the elastic properties of the lithosphere, $F_i(x)$ can be computed with finite element software or with an analytical solution (e.g. *Okada*, 1992; *Meade*, 2007). Likewise, $G_{ij}(x)$ can be computed using finite element software or semi-analytic techniques (e.g. *Pollitz*, 1997; *Barbot & Fialko*, 2010; *Fukahata & Matsu'ura*, 2006) if the assumed geometry of the viscoelastic regions is sufficiently simple. We are left to find the unknown slip parameters, α_{ik}, and unknown viscosities in each region of the lithosphere, η_j.

We estimate these unknown parameters from observations of surface deformation in a least squares sense. Let $\mathbf{u_{obs}}$ be a vector of observed coseismic and postseismic surface displacements at various locations and points in time. Let $\mathbf{m}$ be a vector of all the unknown parameters in α_{ik} and η_j with length $Q = M+N+P$ and let $\mathbf{u}(\mathbf{m})$ be a vector of postseismic surface displacements predicted by eq (20). We seek to solve

$$\min \left|\left| \mathbf{f}(\mathbf{m}) \right|\right|_2^2 \tag{21}$$

subject to the constraint that

$$\mathbf{m} \geq 0, \tag{22}$$

where

$$\mathbf{f}(\mathbf{m}) = \begin{vmatrix} \mathbf{W}\left(\mathbf{u}(\mathbf{m}) - \mathbf{u}_{\text{obs}}\right) \\ \mathbf{Lm} \end{vmatrix}. \tag{23}$$

In the above equation, $\mathbf{W}$ is a diagonal matrix containing the reciprocal of the data uncertainties.

We impose a nonnegativity constraint on $\mathbf{m}$ because it ensures that inferred slip is in one predominant direction. Specifically, it constrains the rake of inferred slip on each fault patch to be between the rake of our chosen basis slip directions. Additionally, the nonnegativity constraint on $\mathbf{m}$ prevents unphysical viscosity inferences.

Because this inverse problem inevitably has nonunique solutions for $\mathbf{m}$, we put additional constraints on the model parameters with the matrix $\mathbf{L}$. In our following synthetic tests we constrain the solution by minimizing the Laplacian of the spatial distribution of fault slip and lithospheric viscosity. We do so by letting $\mathbf{L}$ be the umbrella operator (*Desbrun et al.*, 1999) such that

$$\sum_{j}^{Q} L_{ij} m_j = \frac{\lambda_i}{|\mathcal{N}(i)|} \sum_{k \in \mathcal{N}(i)} m_k - m_i, \tag{24}$$

where $\mathcal{N}(i)$ denotes the set of indices for model parameters describing slip (viscosity) which is adjacent to the slip (viscosity) described by m_i. λ_i is a penalty parameter which controls how much we enforce the smoothness constraint. We allow λ_i to vary based on the model parameters it is smoothing because a constant penalty parameter would cause the fault slip parameters, α_{ik}, to be regularized just as much as the viscosity parameters, η_j. This may not be desirable because viscosity is not as well constrained by postseismic deformation and therefore would require a larger penalty parameter than for the fault slip parameters. Likewise, the parameters in α_{ik} which describe coseismic slip are likely to be better constained than the parameters in α_{ik} describing afterslip. We therefore use 10-fold cross validation to

find an optimal penalty parameters for the coseismic slip parameters, afterslip parameters, and viscosity parameters.

We find $\mathbf{m}$ that satisfies the above conditions with the Gauss-Newton method (e.g. *Aster et al.*, 2013). The best fit model parameters are found by making an initial guess for the solution and then iteratively solving

$$\mathbf{J}(\mathbf{m}^k)\mathbf{m}^{k+1} = -\mathbf{f}(\mathbf{m}^k) + \mathbf{J}(\mathbf{m}^k)\mathbf{m}^k \tag{25}$$

for $\mathbf{m}^{k+1}$. $\mathbf{J}(\mathbf{m}^k)$ is the Jacobian of $\mathbf{f}(\mathbf{m})$ with respect to $\mathbf{m}$ evaluated at $\mathbf{m^k}$. We impose the nonnegativity constraint on $\mathbf{m}$ by solving eq (25) with a nonnegative least squares algoritm (*Lawson & Hanson*, 1995).

We find that it is occasionally necessary to constrain the step size for each iteration of eq. (25) in order to ensure convergence. We do so in a manner akin to the Levenberg-Marquardt algorithm (e.g. *Aster et al.*, 2013). We instead solve

$$\mathbf{J}^*(\mathbf{m}^k)\mathbf{m}^{k+1} = -\mathbf{f}^*(\mathbf{m}^k) + \mathbf{J}^*(\mathbf{m}^k)\mathbf{m}^k \tag{26}$$

for m^{k+1}, where

$$\mathbf{J}^*(\mathbf{m}) = \begin{vmatrix} \mathbf{J}(\mathbf{m}) \\ \kappa\mathbf{I} \end{vmatrix} \tag{27}$$

and

$$\mathbf{f}^*(\mathbf{m}) = \begin{vmatrix} \mathbf{f}(\mathbf{m}) \\ \mathbf{0} \end{vmatrix} \tag{28}$$

where κ controls the step size for each iteration and varies depending on whether the algorithm is converging.

In a nonlinear least squares algorithm, computing the Jacobian typically is the largest computational burden; however in this case, evaluating the Jacobian of eq (20) requires only a few computationally inexpensive matrix operation. Consequently, our nonlinear least squares algorithm converges to a solution for $\mathbf{m}$ in a matter of seconds on a desktop computer. The main computational burden is in computing $F_i(x)$ and $G_{ij}(x)$ which is done with finite element software and only needs to be done once for a given fault and lithosphere geometry.

Throughout this paper, our initial guess for the model parameters is that there is no slip on any fault patch, and the lithosphere is entirely elastic ($1/\eta = 0$). In our experience, the choice of initial guess has an insignificant effect on the best fit solution.

5 Synthetic test

5.1 Synthetic postseismic deformation

We demonstrate with a synthetic test that our inverse method is capable of recovering fault slip and lithospheric viscosity from postseismic deformation. We use the finite element software, Pylith (*Aagard et al.*, 2013), to compute the surface deformation resulting from a specified amount of slip on a fault in a lithosphere with a specified viscosity. We invert this synthetic surface deformation using the method described above to see if we are able to recover the imposed model parameters. The synthetic test also serves to demonstrate that eq. (16) and eq. (18) are indeed valid for three dimensional earthquake models.

Our synthetic model consists of a 50 km long by 20 km wide strike-slip fault striking north and dipping 60° to the east (figure 4). At $t = 0.0$ we impose $6.54 * 10^{19}$ N m of surface rupturing right-lateral coseismic slip with a distribution shown in figure 2. After the coseismic slip, we impose a constant rate of afterslip from $t = 0.0$ to $t = 0.5$ years. The cumulative seismic moment over this interval is about $1.07 * 10^{19}$ N m. The spatial distribution of afterslip is shown in figure 2. During the interval $t = 0.5$ to $t = 1.0$ years the rate of afterslip is decreased by a factor of 2. From $t = 1.0$ year onward, we do not impose

any fault slip.

The lithosphere in our synthetic model is Maxwell viscoelastic with homogenous Lamé parameters $\lambda = 32.0$ GPa and $\mu = 32.0$ GPa. The viscosity in the lithosphere decays from 10^{21} Pa s ($\tau = 1,000$ years) at the surface to 10^{19} Pa s ($\tau = 10$ years) at 75 km depth (figure 3). We compute displacements at 0.1 year intervals up until $t = 10$ years, which makes our chosen upper bound on viscosity effectively elastic on these timescales.

We compute surface displacements at 60 randomly chosen locations within a 400 km square centered about the fault (figure 4). This is intended to roughly correspond with the density of GPS station at a well instrumented plate boundary.

Additionally, we add noise to our displacements which is consistent with what one would expect from GPS observations. The noise is temporally correlated with a characteristic timescale of 0.25 years. The temporal covariance is intended to simulate seasonal processes which are typically present in GPS timeseries. The standard deviation of northing and easting displacements is 1.0 mm, and the standard deviation of the vertical displacements is 2.5 mm.

5.2 Green's functions

We invert the synthetic surface deformation for fault slip on a 4 km by 4 km discretization of the synthetic fault segment and we estimate viscosity in 10 km thick horizontal layers from the surface down to 70 km depth.

We compute the elastic Green's functions, $F_i(x)$, and instantaneous viscous Green's functions, $G_{ij}(x)$, numerically using Pylith. The elastic Greens functions are the initial displacements resulting from 1.0 m of imposed slip on fault patch i. For each fault patch we compute the elastic Green's functions for slip with rake 45° updip and 45° downdip of pure right-lateral slip. This restricts all inferred slip to be withing 45° of right-lateral. We compute the initial viscoelastic Green's functions by setting the lithosphere to be elastic everywhere except in region j, which is assigned a viscosity of 10^{18} Pa s. We then impose 1.0 m of slip on fault

patch i and use the computed initial rates of surface deformation as $G_{ij}(x)$.

We define the basis slip functions, $A_k(t)$, as a heaviside function centered at $t = 0.0$ and three ramp functions which increase from 0.0 to 1.0 m of slip over the time intervals $0.0 \leq t < 0.5$ years, $0.5 \leq t < 1.0$ years, and $1.0 \leq t < 10.0$ years. Although our synthetic model does not have any fault slip during the last time interval, we include it to test if postseismic deformation over that interval, which is resulting purely from viscous creep, can be describe with continued fault slip.

5.3 Recovered model

Our best fitting model of slip on the fault is shown in figure 2. The spatial distribution, direction, and magnitude of our inferred coseismic slip is a good match to the synthetic coseismic slip. This is not surprising given that the magnitude of coseismic displacments is far larger than the magnitude of the added noise.

The surface displacements over the intervals $0.0 < t < 0.5$ years and $0.5 < t < 1.0$ years are an order of magnitude smaller than the coseismic displacements and so the postseismic signal is more obscured by the added noise. Consequently, we are not able to accurately recover the spatial distribution of afterslip on the fault over these time intervals. However, the seismic moment of inferred afterslip is consistent with the seismic moment in the synthetic model meaning that the total amount of afterlip is well recovered but is largely smoothed out over the fault plane by the regularization. Our recovered model is therefore accurately attributing deformation during this time interval to afterslip rather than viscous deformation. We note that lowering the penalty parameter for afterlip would result in a spatial distribution of afterslip that is more consistent with the afterslip in the synthetic model and it is possible that our recovered afterslip would be better recovered using a method other than 10-fold cross validation to find our penalty parameters.

The inferred slip over the last time interval, 1.0 to 10.0 years following the earthquake, is also consistent with the synthetic model. The seismic moment of slip over this interval is

$5 * 10^{17}$ N m, which is two orders of magnitude smaller than the moment for the coseismic slip. This means that the inferred slip is accounting for, at most, a few mm's of displacement from $t = 1.0$ to $t = 10.0$ years. This is on order of the data uncertainty and so the inferred slip is negligably small.

The inferred viscosities in each of the eight layers are shown in figure 3a. The recovered viscosities correspond well with the synthetic model except perhaps for the top layer from 0 to 10 km depth. We used bootstrapping to estimate the uncertainties of the recovered viscosities and we found that the strongest layers near the surface, despite being proximal to the earthquake source, have the highest uncertanties. However, viscosities greater than 10^{20} Pa s are effectively elastic on the timescales of this synthetic test and so a wide range of high viscosities for the upper layers would just as adequately be able to describe the synthetic surface displacements. When looking at inferred values of fluidity (figure 3b), we see that the uncertainties are lowest at the surface and increase with depth, as is perhaps more intuitive.

5.4 solution validation

The fact that our recovered fault slip and lithospheric viscosity are in good agreement with the synthetic model suggests that the approximation given by eq. (18) is accurate over the ten years of synthetic data. We quantify the accuracy of eq. (18) by running a forward model with Pylith where the imposed fault slip and lithospheric viscosity are those found in our recovered model. We then compare the displacements from the numerically computed forward model with the displacements predicted by eq. (18). We refer to the numerically computed displacements as $\mathbf{u}_{\text{true}}(t)$ and the displacments predicted by our approximation as $\mathbf{u}(t)$. We define the approximation residuals as $\mathbf{u}(t) - \mathbf{u}_{\text{true}}(t)$.

Figure 7 shows a map view of the approximation residuals at $t = 10.0$ and $t = 20.0$ years. The approximation residuals at $t = 10.0$ years are small (mm's) compared to the magnitude of displacements at this time (cm's), indicating that eq. (18) is indeed a fair approximation over these timescales. The validity of eq. (18) is clearly demonstrated in figure 5, which

shows $\mathbf{u}(t)$ and $\mathbf{u}(t)_{\text{true}}$ at a sample site near the fault. The numerical solution asymptotically approaches the rate of deformation predicted by eq. (18) as the time goes to zero, which demonstrates the validity of eq. (16). The approximation begins to notably diverge from the numerical solution about 10 years after the earthquake.

Figure 7 also shows the root mean square error as a function of time which we define as

$$\text{RMSE}(t) = \frac{||\mathbf{u}(t) - \mathbf{u}_{\text{true}}(t)||_2}{\sqrt{\text{R}}}, \tag{29}$$

where R is the number of elements in $\mathbf{u}(t)$ and $\mathbf{u}_{\text{true}}(t)$. The root mean square error describes how much we would expect the approximate displacements to deviate from the true displacements for a given time. Generally speaking, our approximation can be considered reasonably accurate when the root mean square error is lower than the observation uncertainty. The RMSE increases quadratically from 0 at $t = 0$ to a few millimeters at $t = 20$. When considering that noise for geodetic observations is also on order of a few millimeters, this approximation appears to be sufficiently accurate for at least up until $t = 10$ years.

6 Discussion

Our method for estimating slip and viscosity from postseismic deformation makes the assumption that the timescale of relaxation in the lithosphere is greater than or about equal to the timescales over which postseismic deformation is observed. Since the lithosphere's relaxation time is generally not well known, there is the added complication of deciding how much of a postseismic timeseries to use in the above described inverse method. We conveniently picked the length of our timeseries to correspond with the weakest relaxation time in the lithosphere; however, the length of the timeseries could have also been determined iteratively. If the approximation given by eq. (18) is incapable of adequately describing obersvations, then it is likely that the timeseries used in the inversion is too long. One can reduce the length of the postseismic timeseries used in the inversion until an adequate fit is

found.

Our synthetic data is characterized by transient near field surface deformation followed by a steady rate of more diffuse surface deformation. This is qualitatively similar to postseismic deformation following other large ($\geq$ Mw7) earthquakes ((*Pollitz*, 2003, 2005; *Ryder et al.*, 2007; *Rollins et al.*, 2015)). Some have sought to explain this pattern of surface deformation using a more complex lithospheric rheology capable of transient deformation. We suggest alternatively that fault creep and a relatively high viscosity lithosphere would also be capable of describing the commonly observed patterns of postseismic deformation. In such case, our method described here would allow us to easily constrain the amount of slip and the lithospheric viscosity necessary to describe observed postseismic deformation

Laboratory studies suggest that the lithospheres rheology is generally nonlinear with respect to stress, contradicting our assumption that the lithosphere is Maxwell viscoelastic. However, the above described approximation assumes that stresses in the lithosphere are not significantly different from the stresses induced from fault slip. Under the assumption of constant stress, a material with a nonlinear rheology will behave as a Maxwell viscoelastic material and it will have an effective Maxwell viscosity. This means that viscosities inferred using the above inverse method can be instead interpretted as the effective Maxwell viscosities for the current state of stress in the lithosphere.

Discuss how the solution found here can be used as a first step in a nonlinear least squares algorithm where the forward problem requires using a FEM rather than eq. 18

7 Conclusion

A Inverse Laplace transorm through series expansion

let $f(t)$ and all of its derivatives be continuous and bounded such that there exists a real valued M_o, C_o and t_o that satisfies

$$f^{(n)}(t) < C_o e^{M_o t} \ \forall \ t > t_o. \tag{30}$$

The Laplace transform of $f(t)$ is defined as

$$\mathcal{L}[f(t)] := \hat{f}(s) := \int_0^\infty f(t) e^{-st} dt. \tag{31}$$

Our imposed bounds on $f^{(n)}(t)$ ensures that

$$\lim_{s\to\infty} \mathcal{L}[f^{(n)}(t)] = 0. \tag{32}$$

It can be easily shown using integration by parts that

$$\mathcal{L}[f^{(n)}(t)] = s^n \hat{f}(s) - \sum_{m=1}^{n} s^{m-1} f^{(n-m)}(0). \tag{33}$$

Substituting eq. (33) into eq. (32) and then rearranging the terms gives us a recursive formula for $f^{(n)}(0)$ in terms of $\hat{f}(s)$:

$$f^{(n)}(0) = \begin{cases} \lim_{s\to\infty} \left(s\hat{f}(s)\right), & \text{if } n = 0 \\ \lim_{s\to\infty} \left(s^{n+1}\hat{f}(s) - \sum_{m=0}^{n-1} s^{m+1} f^{(n-m-1)}(0)\right), & \text{if } n > 0 \end{cases} \tag{34}$$

We can use eq. (34) to construct a Taylor series expansion of $f(t)$ about $t = 0$,

$$f(t) = \sum_{n=0}^{\infty} \frac{f^{(n)}(0)}{n!} t^n. \tag{35}$$

Since $f^{(n)}(0)$ can be expressed entirely in terms of $\hat{f}(s)$, evaluating the above series expansion is effectively the same as performing an inverse Laplace transform on $\hat{f}(s)$.

References

Fukahata, Y., Matsuura, M., 2006. Quasi-static internal deformation due to a dislocation source in a multilayered elastic/viscoelastic half-space and an equivalence theorem. *Geophys. J. Int.*, 166, 418-434. doi:10.1111/j.1365-246X.2006.02921.x.

Pollitz, F.F., 1997. Gravitational viscoelastic postseismic relaxation on a layered spherical Earth. *J. Geophys. Res.*, 102, 17921-17941. doi:10.1029/97JB01277.

Barbot, S. & Fialko, Y., 2010. A unified continuum representation of post-seismic relaxation mechanisms: Semi-analytic models of afterslip, poroelastic rebound and viscoelastic flow, *Geophys. J. Int.*, 182, 1124-1140. doi:10.1111/j.1365-246X.2010.04678.x.

Meade, B.J., 2007. Algorithms for the calculation of exact displacements, strains, and stresses for triangular dislocation elements in a uniform elastic half space, *Computers and Geosciences*, 33, 1064-1075. doi:10.1016/j.cageo.2006.12.003.

Okada, Y., 1992. Internal deformation due to shear and tensile faults in a half space, *Bull. Seismol. Soc. Am.*, 82, 1018-1040.

Johnson, K.M., Bürgmann, R. & Freymueller, J.T., 2009. Coupled afterslip and viscoelastic flow following the 2002 Denali Fault, Alaska earthquake. *Geophys. J. Int.*, 176, 670-682. doi:10.1111/j.1365-246X.2008.04029.x.

Freed, A.M., Bürgmann, R., Calais, E., Freymueller, J. & Hreinsdóttir, S., 2006. Implications of deformation following the 2002 Denali, Alaska, earthquake for postseismic relaxation processes and lithospheric rheology. *J. Geophys. Res. Solid Earth*, 111, 1-23. doi:10.1029/2005JB003894.

Hsu, Y.-J., Simons, M., Avouac, J.-P., Galetzka, J., Sieh, K., Chlieh, M., Natawidjaja, D., Prawirodirdjo, L. & Bock, Y., 2006. Frictional Afterslip Following the 2005 Nias-Simeulue Earthquake, Sumatra, *Science*, 312, 1921-1926.

Desbrun, M., Meyer, M., Schröder, P. & Barr, A.H., 1999. Implicit fairing of irregular meshes using diffusion and curvature flow, *Proceedings of the 26th Annual Conference on Computer Graphics and Interactive Techniques*, 317324. doi:10.1145/311535.311576.

Ryder, I., Parsons, B., Wright, T.J. & Funning, G.J., 2007. Post-seismic motion following the 1997 Manyi (Tibet) earthquake: InSAR observations and modelling, *Geophysical Journal International*, 169, 10091027. doi:10.1111/j.1365-246X.2006.03312.x.

Hetland, E.A. & Hager B.H., 2003. Postseismic relaxation across the Central Nevada Seismic Belt, *Journal of Geophysical Research*, 108, 113. doi:10.1029/2002JB002257.

Pollitz, F.F., 2005. Transient rheology of the upper mantle beneath central Alaska inferred from the crustal velocity field following the 2002 Denali earthquake, *Journal of Geophysical Research: Solid Earth*, 110, 116. doi:10.1029/2005JB003672.

Hetland, E.A. & Hager, B.H., 2005. Postseismic and interseismic displacements near a strike-slip fault: A two-dimensional theory for general linear viscoelastic rheologies. *J. Geophys. Res. Solid Earth*, 110, 1-21. doi:10.1029/2005JB003689.

Bürgmann, R., Ergintav, S., Segall, P., Hearn, E.H., McClusky, S., Reilinger, R.E., Woith, H. & Zschau, J., 2002. Time-dependent distributed afterslip on and deep below the İzmit earthquake rupture, *Bull. Seismol. Soc. Am.*, 92, 126-137. doi:10.1785/0120000833.

Harris, R.A. & Segall, P., 1987. Detection of a locked zone at depth on the Parkfield, California, segment of the San Andreas Fault. *J. Geophys. Res.*, 92, 7945-7962. doi:10.1029/JB092iB08p07945.

Jónsson, S., Segall, P., Pedersen, R. & Bjornsson, G., 2003. Post-earthquake ground movements correlated to pore-pressure transients, *Nature*, 424, 179-183. doi:10.1038/nature01758.1.

Peltzer, G., Rosen, P., Rogez, F. & Hudnut, K., 1998. Poroelastic rebound along the Landers 1992 earthquake surface rupture. *J. Geophys. Res.*, 103, 30131-30145. doi:10.1029/98JB02302.

Pollitz, F.F., 2003. Transient rheology of the uppermost mantle beneath the Mojave Desert, California, *Earth Planet Sci. Lett.*, 215, 89-104. doi:10.1016/S0012-821X(03)00432-1.

Riva, R.E.M. & Govers, R., 2009. Relating viscosities from postseismic relaxation to a realistic viscosity structure for the lithosphere. *Geophys. J. Int.*, 176, 614-624. doi:10.1111/j.1365-246X.2008.04004.x.

Hines, T.T. & Hetland, E.A., 2013. Bias in estimates of lithosphere viscosity from interseismic deformation, *Geophys. Res. Lett.*, 40, 4260-4265. doi:10.1002/grl.50839.

Rollins, C., Barbot, S. & Avouac, J-P. 2015, Postseismic Deformation Following the 2010 Mw7.2 El Mayor-Cucapah Earthquake: Observations, Kinematic Inversions, and Dynamic Models, *Pure Appl. Geophys.*, doi:10.1007/s00024-014-1005-6.

Marone, C.J., Scholz, C.H. & Bilham, R., 1991. On the mechanics of earthquake afterslip, *J. Geophys. Res.*, 96, 8441-8452.

Barbot, S., Fialko, Y. & Bock, Y., 2009. Postseismic deformation due to the Mw 6.0 2004 Parkfield earthquake: Stress-driven creep on a fault with spatially variable rate-and-state friction parameters, *J. Geophys. Res. Solid Earth*, 114, 1-26. doi:10.1029/2008JB005748.

Freed, A.M., 2007. Afterslip (and only afterslip) following the 2004 Parkfield, California, earthquake, *Geophys. Res. Lett.*, 34, 1-5. doi:10.1029/2006GL029155.

Segall, P., 2010. Earthquake and volcano deformation, pp 185-186, Princeton University Press.

Hearn, E.H., McClusky, S., Ergintav, S. & Reilinger, R.E., 2009. İzmit earthquake postseismic deformation and dynamics of the North Anatolian Fault Zone. *J.Geophys. Res. Solid Earth*, 114, 1-21. doi:10.1029/2008JB006026.

Flügge, W., 1975. Viscoelasticity, Springer-Verlag Berlin Heidelberg.

Lawson, C.L. & Hanson, R.J., 1995. Solving least Squares Problems, SIAM.

Chinnery, M.A. & Jovanovich, D.B., 1972. Effect of earth layering on earthquake displacement fields, *Bull. Seismol. Soc. Am.*, 62, 1629-1639.

Rybicki, K., 1971. The elastic residual field of a very long strike-slip fault in the presence of a discontinuity, *Bull. Seism. Soc. Am.*, 61, 79-92.

Nur, A. & Mavko, G., 1974. Postseismic Viscoelastic Rebound, *Science*, 183, 204-206. doi:10.1126/science.183.4121.204.

Savage, J. & Prescott, W., 1978. Asthenosphere readjustment and the earthquake cycle, *J. Geophys. Res.*, 83, 3369-3376.

Aster, R.C., Borchers, B., Thurber, C.H., 2013. Parameter estimation and inverse problems, *Academic Press*.

Aagaard, B.T., Knepley, M.G. & Williams, C.A., 2013. A domain decomposition approach to implementing fault slip in finite-element models of quasi-static and dynamic crustal deformation, *Journal of Geophysical Research: Solid Earth*, 118, doi: 10.1002/jgrb.50217.

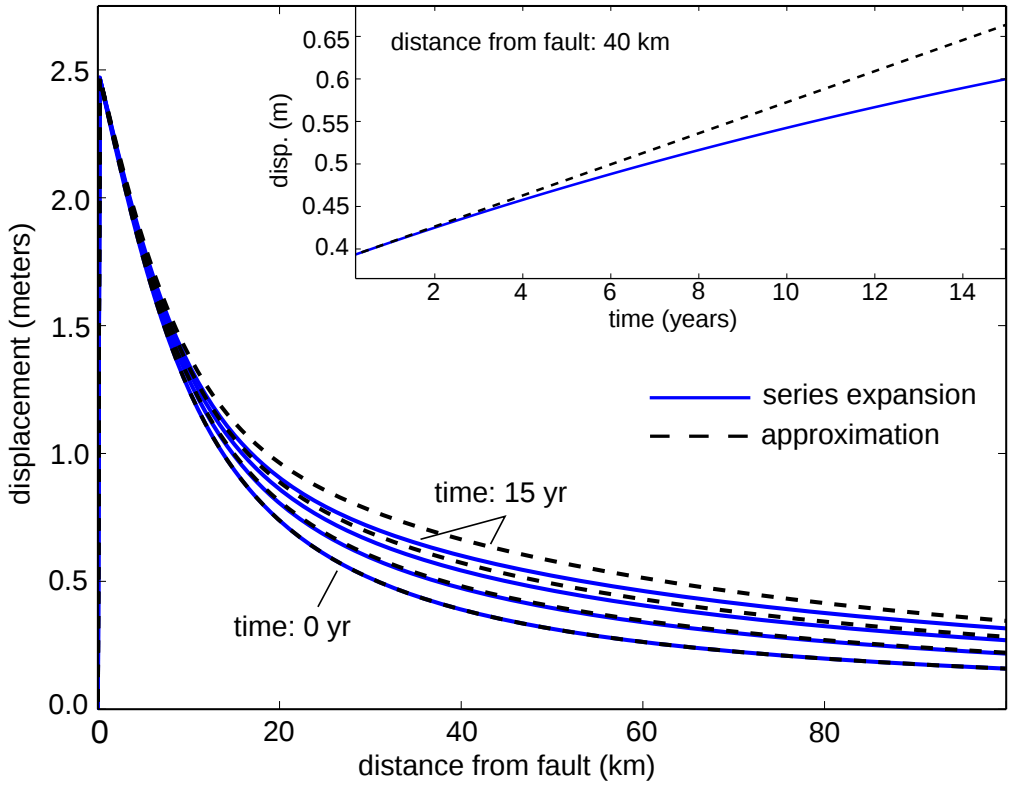

Figure 1: Surface displacements predicted by eq. (11) truncated after five terms (blue) and the approximation given by eq. (12) (dotted black). Displacements are shown at times 0, 5, 10, and 15 years following an earthquake

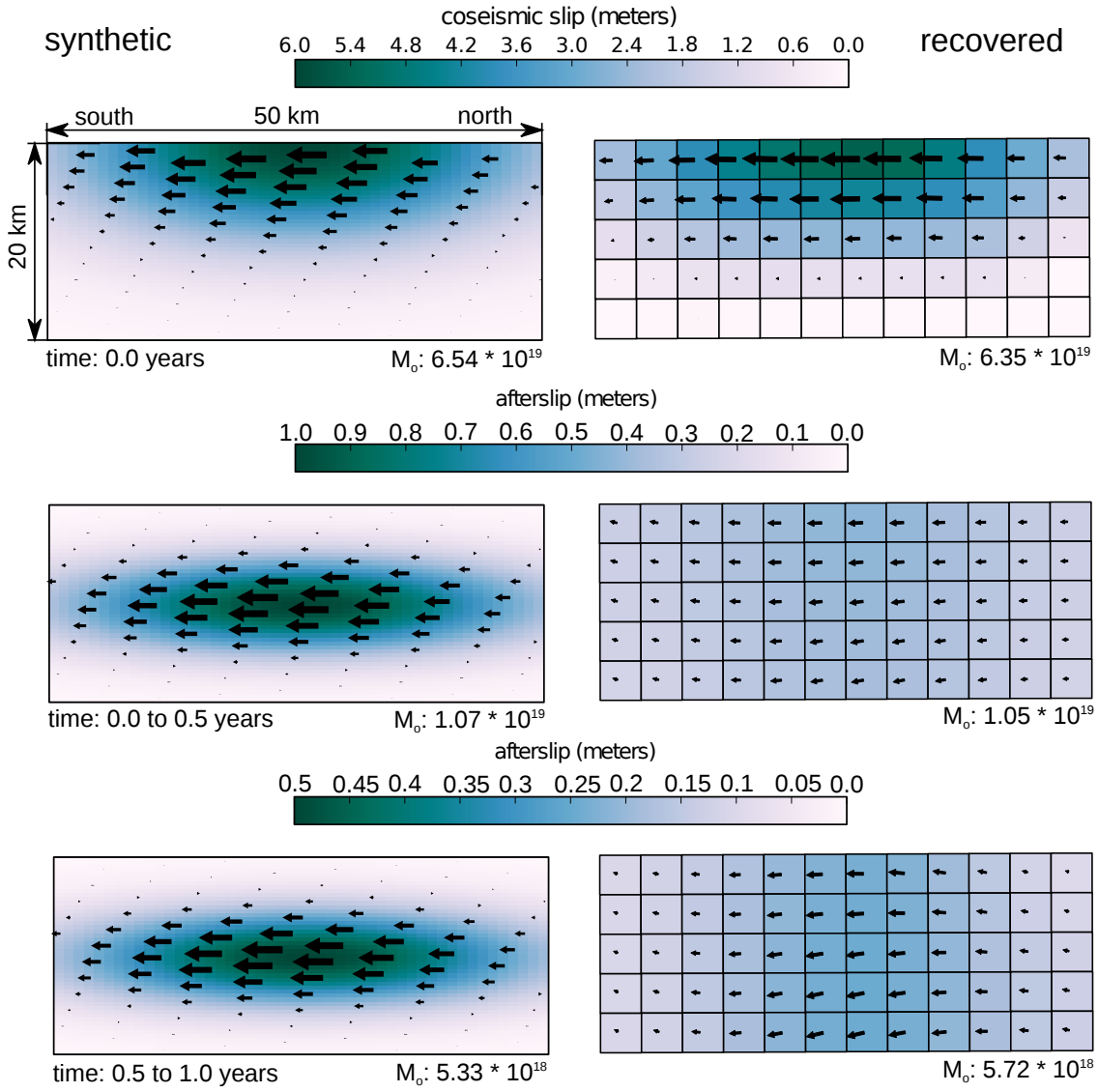

Figure 2: Left: slip distribution imposed in the synthetic model. The panels from top to bottom represent coseismic slip at time = 0.0, and afterslip over the period 0.0 to 0.5 years, 0.5 to 1.0 years, and 1.0 to 10.0 years. Colors indicate magnitude of slip and arrows indicate direction of slip. Right: Slip recovered from inverting the synthetic surface deformation.

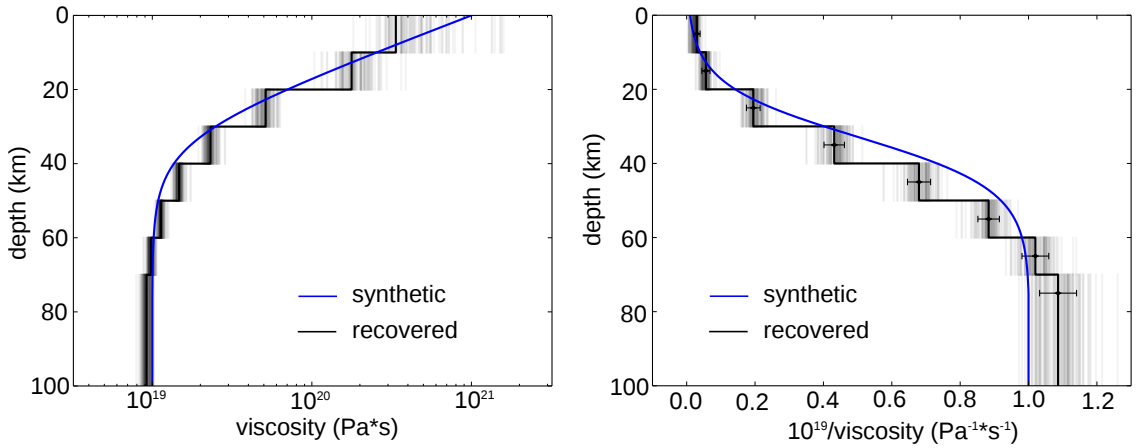

Figure 3: Synthetic and recovered lithospheric viscosity strucutures. Blue line indicates viscosity structure imposed in the synthetic test. Black line indicates viscosity structure inferred from the synthetic surface displacement. Semi-transparent lines are recovered models found through bootstrapping and indicate the degree of uncertainty on the inferred viscosity structure. The left and right panels show the same information under different projections

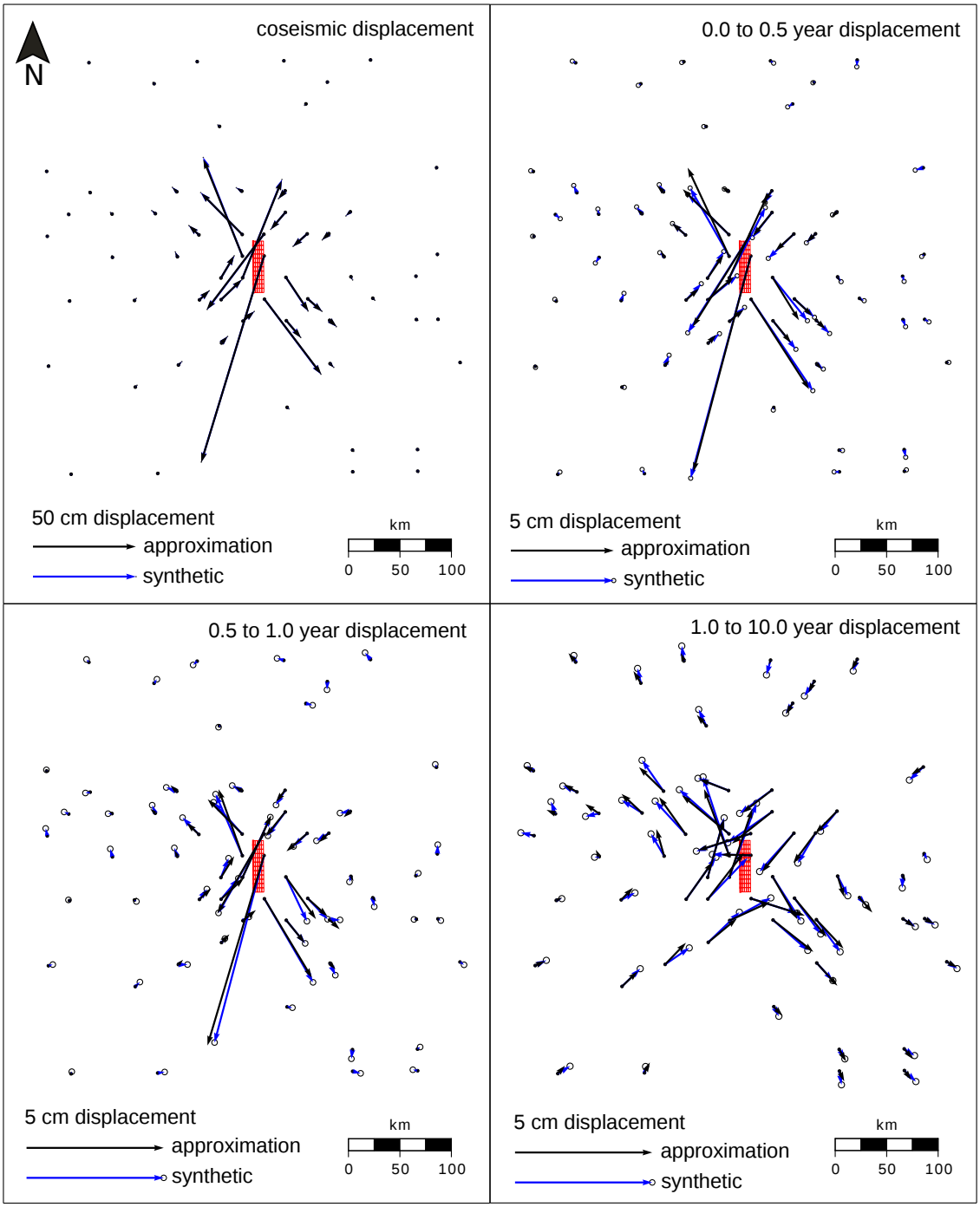

Figure 4: Synthetic surface displacements (blue) and best fitting surface displacements (black). Vertical displacements are used in the inversion but are not shown here. The top left panel shows coseismic displacements and the remaining panals show the displacements over the indicated time intervals. Red dot indicates the position whos time series is shown in figure 5. The red wireframe is the synthetic fault discretized into fault patches.

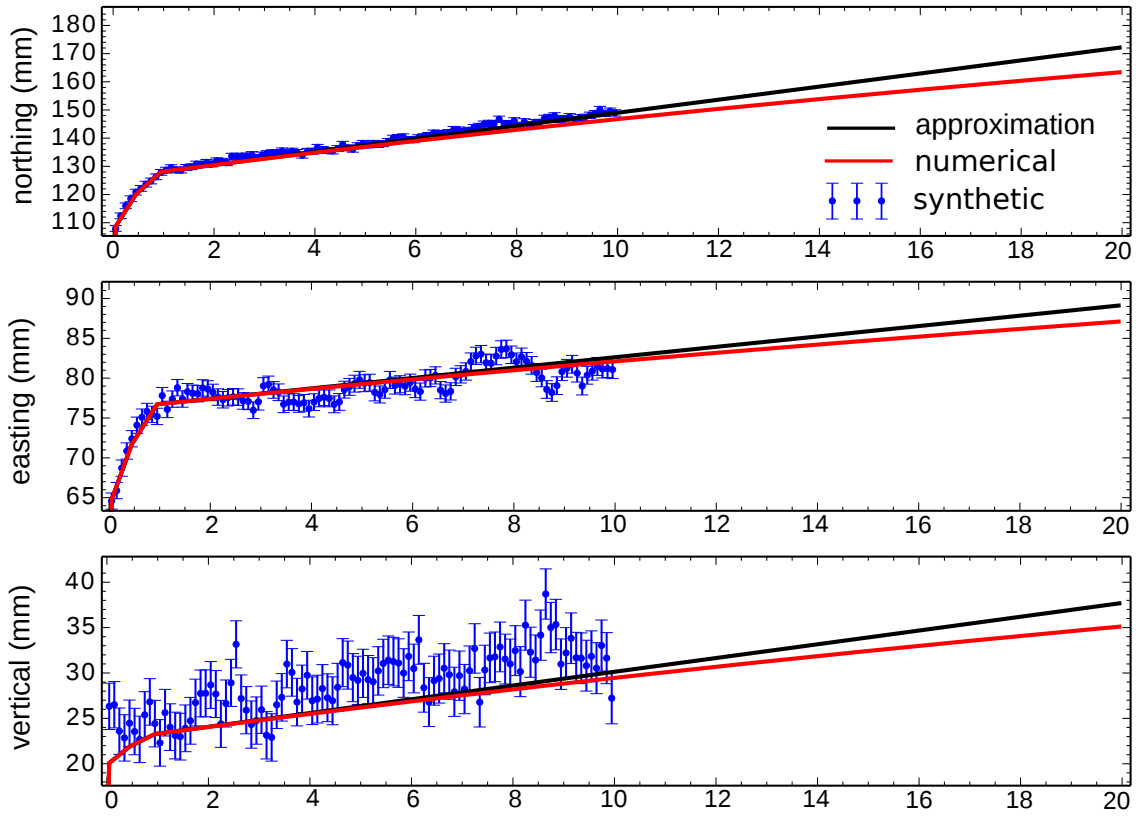

Figure 5: Displacement time series for the position shown in figure 4 (blue) and best fitting surface displacements using the approximation from eq. (18) (black). The red line indicates surface displacements computed using Pylith where the inferred slip distribution and viscosity structure are used as input. Values for displacement are with respect to the locations preseismic position.

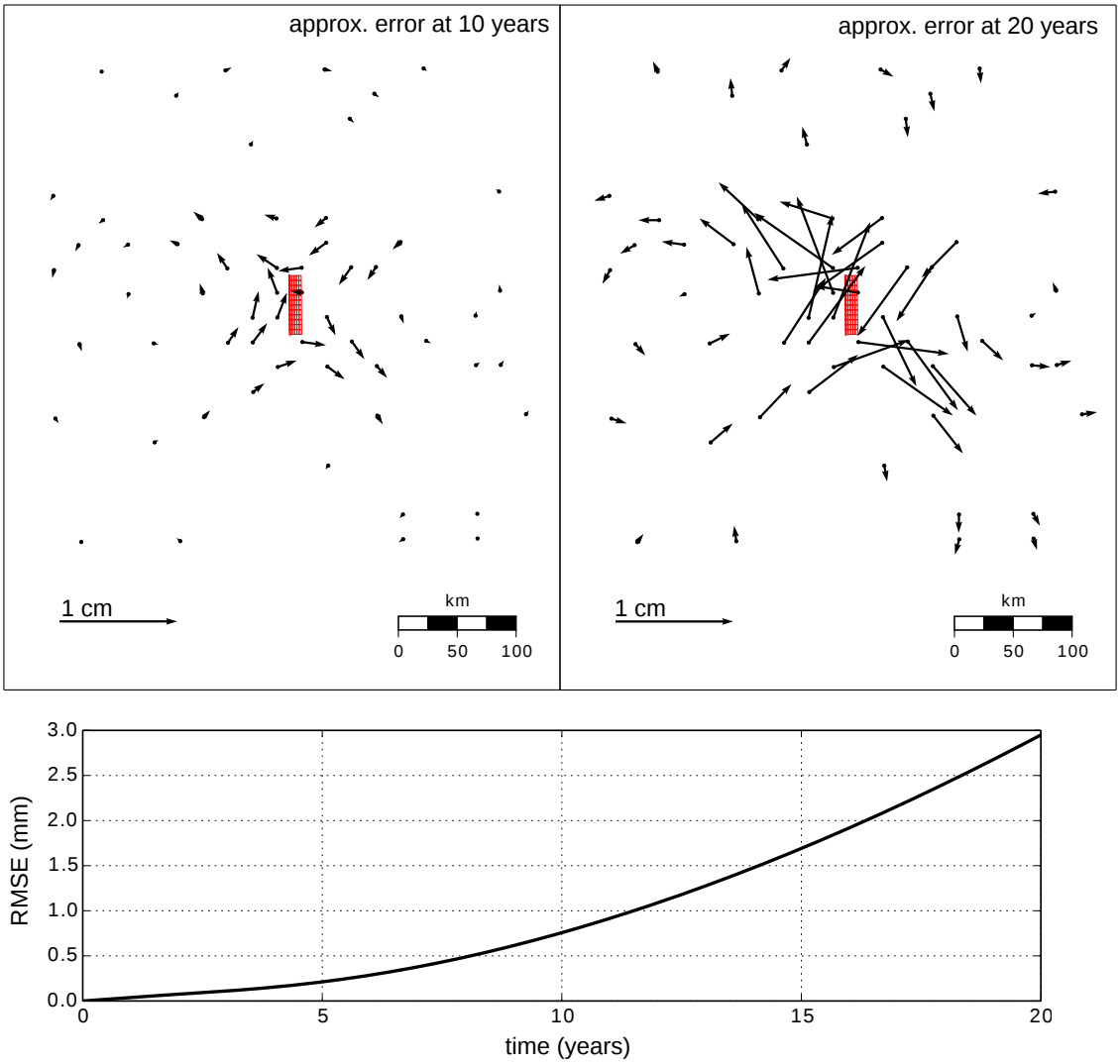

Figure 6: Difference between the surface displacement approximation and the numerically computed surface displacements. Top left panel shows the difference 10 years after the earthquake and the top right panel shows the difference at 20 years. The bottom panel shows the root mean square of the approximation error over time.